

## PROPERTIES OF THE DIFFUSE EMISSION AROUND WARM LOOPS IN SOLAR ACTIVE REGIONS

DAVID H. BROOKS<sup>1,2</sup>

<sup>1</sup>College of Science, George Mason University, 4400 University Drive, Fairfax, VA 22030  
*Draft version January 24, 2019*

### ABSTRACT

Coronal loops in active regions are the subjects of intensive investigation, but the important diffuse 'unresolved' emission in which they are embedded has received relatively little attention. Here we measure the densities and emission measure (EM) distributions of a sample of background-foreground regions surrounding warm (2 MK) coronal loops, and introduce two new aspects to the analysis. First, we infer the EM distributions only from temperatures that contribute to the same background emission. Second, we measure the background emission co-spatially with the loops so that the results are truly representative of the immediate loop environment. The second aspect also allows us to take advantage of the presence of embedded loops to infer information about the (unresolvable) magnetic field in the background. We find that about half the regions in our sample have narrow but not quite isothermal EM distributions with a peak temperature of 1.4–2 MK. The other half have broad EM distributions (Gaussian width  $>3 \times 10^5$  K), and the width of the EM appears to be correlated with peak temperature. Densities in the diffuse background are  $\log(n/\text{cm}^{-3}) = 8.5\text{--}9.0$ . Significantly, these densities and temperatures imply that the co-spatial background is broadly compatible with static equilibrium theory (RTV scaling laws) provided the unresolved field length is comparable to the embedded loop length. For this agreement to break down, the field length in most cases would have to be substantially longer than the loop length, a factor of 2–3 on average, which for our sample approaches the dimensions of only the largest active regions.

*Subject headings:* Sun: corona—Sun: activity—Sun: UV radiation—Techniques: spectroscopic

### 1. INTRODUCTION

Solar active regions typically comprise a hot ( $\sim 4$  MK) core, surrounded by higher lying warm ( $\sim 1.7$  MK) loops, and peripheral cooler fan structures ( $\sim 1$  MK). The whole region is embedded in diffuse unresolved emission from the foreground and background around loops. Understanding the physical properties of these structures is key to providing constraints on theories of how they are heated.

There is a vast literature on measurements of the temperatures and densities of coronal loops. Reale (2014) gives a very comprehensive review. One specific issue that has attracted a great deal of attention over the years is whether coronal loops are consistent with static equilibrium theory and therefore whether they are heated steadily or impulsively. Observations of high temperature soft X-ray loops from the *Yohkoh* satellite by Porter & Klimchuk (1995) appeared to show that these loops last longer than the expected radiative and conductive cooling time and that they are therefore heated in a quasi-steady fashion. Measurements of the temperatures, pressures, and lengths also showed that the loops are consistent with the static equilibrium scaling laws derived by Rosner et al. (1978). Consistency with static equilibrium theory is now thought to indicate that loops are heated quasi-steadily by high frequency impulsive heating (Klimchuk 2006). Measurements of intensities, Doppler, and non-thermal velocities at the footpoints of active region core loops from the *Hinode* EUV Imaging Spectrometer (EIS, Culhane et al. 2007) also do not show much variation over many hours (Brooks & Warren 2009), and the emission measure (EM) distributions at the loop apex are often narrow with a steep slope (Warren et al. 2011; Winebarger et al. 2011). These results imply that they are not evolving through

a broad range of temperatures (Warren et al. 2012), though there is evidence that the EM slope varies within a single AR (Del Zanna et al. 2015), between others (Tripathi et al. 2011), and as a function of AR age (Ugarte-Urra & Warren 2012). Furthermore, intensity time-lag analysis shows that these loops are partially cooling and being re-heated at high temperatures (Viall & Klimchuk 2017). Higher spatial and temporal resolution observations also detect variability on shorter time-scales (Testa et al. 2013), though this may depend on the initial conditions in the heated loop (Polito et al. 2018).

The warm loops formed at lower temperatures also persist longer than expected cooling times (Lenz et al. 1999), and the majority have narrow, near isothermal temperature distributions (Del Zanna 2003; Aschwanden & Nightingale 2005; Warren et al. 2008). In contrast to the hot core loops, however, the warm loops are clearly over-dense compared to static equilibrium theory (Lenz et al. 1999; Aschwanden et al. 2001; Winebarger et al. 2003).

It was recognized early on that emission from the background/foreground complicates the analysis of coronal loops (Klimchuk et al. 1992). Del Zanna & Mason (2003) argue that background subtraction is essential for obtaining accurate measurements. This is because the background emission itself can account for  $>70\%$  of the intensity measured along the line-of-sight towards the loop (Del Zanna & Mason 2003; Aschwanden & Nightingale 2005; Brooks et al. 2012), though this may be reduced in higher spatial resolution observations (Del Zanna 2013). Such a large contribution clearly has a significant potential impact on the derived properties of loops. For one, when determining the thermal distribution, it makes it difficult to determine whether weak emission at the low- and high-temperature extremes is actually coming from the same loop structure. This is often handled by only including the emission from spectral lines with cross-

<sup>2</sup> Current address: Hinode Team, ISAS/JAXA, 3-1-1 Yoshinodai, Chuo-ku, Sagami-hara, Kanagawa 252-5210, Japan

loop intensity profiles that are correlated (Warren et al. 2008). Background removal techniques, however, and the locations where the background is measured, also have a significant influence on results. Aschwanden et al. (2008) report that the thermal width of warm loops varies with the proximity of the loop to the location where the background is measured. Schmelz et al. (2001) point out that different methods of background subtraction can even result in different conclusions on the location of heating in the same loop (Priest et al. 1998; Aschwanden 2001; Reale 2002). For the higher temperature core loops, background subtraction reduces the amount of lower temperature emission, leading to steeper EM slopes (Del Zanna et al. 2015).

Despite the widespread prevalence and large contribution of this diffuse emission, and therefore its importance in understanding active region and coronal heating, the properties of the background itself have been relatively less studied than those of coronal loops, and those detailed studies that have been made have tended to focus on only a few examples. Del Zanna & Mason (2003) measured EM distributions in the diffuse background adjacent to and within about  $10''$  or so of the leg of a 0.7–1.1 MK isothermal loop observed by the *SOHO* Coronal Diagnostic Spectrometer (CDS, Harrison et al. 1995). They found fairly flat EM distributions (not isothermal) in the 1–2 MK range and electron densities below  $\log(n/\text{cm}^{-3}) = 9$ . Cirtain et al. (2006) examined radial intensity profiles in the background emission above three ARs observed at the limb by CDS and TRACE (Transition Regions And Coronal Explorer, Handy et al. 1999). They found that for the quiescent ARs they studied, the off-limb radial intensity profiles were consistent with an isothermal hydrostatic corona. In contrast, Del Zanna (2012) found a multi-thermal EM distribution peaking at  $\sim 2$  MK for an area of background emission about  $50''$  above the limb and close to an AR observed by EIS. Subramanian et al. (2014) also used EIS data to examine the diffuse emission at  $\sim 2.2$  MK a few tens of arcseconds above two limb active regions in an attempt to clearly isolate it from the hot loops at these temperatures. They found peak temperatures of 1.8 MK and also derived densities below  $\log(n/\text{cm}^{-3}) = 9$  for all the regions they analyzed. Taking a different approach, Viall & Klimchuk (2011) applied their novel intensity time-lag analysis to observations of a location of diffuse emission in an AR core observed by the Atmospheric Imaging Assembly (AIA, Lemen et al. 2012) on the *Solar Dynamics Observatory* (SDO, Pesnell et al. 2012), and concluded that it was consistent with a long duration storm of low-frequency (impulsive) heating. Later, Viall & Klimchuk (2012) studied the diffuse emission in a whole AR and found evidence of widespread cooling and evolution of the plasma. Del Zanna (2013) also has an interesting discussion of the effects of the increased spatial resolution of AIA on the background intensities measured by EIS. He showed that an almost factor of 2 increase in background emission in the core of an AR is likely due to its lower spatial resolution.

Given what we now know about the analysis of coronal loops, there are a number of important issues that should be addressed before we can reliably conclude what the properties of the background emission are. Del Zanna et al. (2015) point out that the slope of the EM distribution for hot loops in the AR core is increased when the background emission is removed, and, as discussed above, we know that the width of the thermal distribution for warm loops is strongly affected by how close to the loop the background is measured (Aschwanden et al. 2008). We also know that it is difficult to

incorporate weak emission at temperatures far removed from the peak temperature and it is not always clear whether it is coming from the same structure and should be included or excluded. This clearly affects the width of the thermal distribution. So a focused analysis of the background emission should consider two important questions.

First, are the properties of the background emission measured adjacent to loops, or of diffuse emission high above and remote from loops, representative of the background in which the loop itself is embedded? Referring again to the discussion by Del Zanna (2013), the increase in background emission in the AR core compared to the periphery (about  $80''$  away), suggested as being due to the lower spatial resolution of EIS compared to AIA, is much larger than what is seen over the much shorter distances (a few arcsecs) across the loops themselves (see Del Zanna (2013) Fig. 8).

Second, does including the emission from spectral lines at all temperatures result in a truly representative EM distribution for the background emission?

In this paper we attempt to address these questions by developing coronal loop analysis techniques to be applied to the background emission. First, we measure the diffuse emission simultaneously and co-spatially with a sample of warm coronal loops, so that it is truly representative of the background in which they are embedded. Second, we introduce a technique that examines the spatial correlation between background intensities in different spectral lines to determine whether the emission at different temperatures is coming from the same structures.

Our analysis and results refine those of previous studies and allow further potentially interesting insights. For example, the densities reported in the background emission are somewhat lower than found in warm loops ( $\log(n/\text{cm}^{-3}) > 9$ , Brooks et al. 2012), so there is a question as to whether the diffuse emission could be compatible with static equilibrium theory? Subramanian et al. (2014) discuss the slopes of the EM distributions in the diffuse emission regions they analyzed and find that they are consistent with both low- and high-frequency heating, and show characteristics that are broadly similar to those of the high temperature core loops. It is difficult to make a direct comparison with loop scaling laws, however, because the lengths of the field lines cannot be determined in the unresolved emission. By measuring the background co-spatially with loops in our work, we are able to make a comparison with static loop scaling laws assuming the background field length is comparable to the length of the loop embedded in it. We also discuss the implications of a breakdown in this assumption. Some very preliminary results from this analysis appeared in Winebarger (2012).

## 2. DATA PROCESSING AND METHODS

We use the sample of 20 warm loops that was previously analyzed by Brooks et al. (2012), supplemented with 4 additional off-limb cases. Since line-of-sight superposition may be less at the limb, we wanted to verify consistent behavior there, but no examples were included in the original sample. Using the same calibration and analysis techniques as in Brooks et al. (2012), we verified that the physical properties (temperature, density) of the new loops fall within the range of values found in the original sample. The Brooks et al. (2012) sample come from EIS raster scans of several active regions present on the solar disk during 2011, and that study provides a detailed analysis of the physical properties of the loops, and comparisons between parameters such as inten-

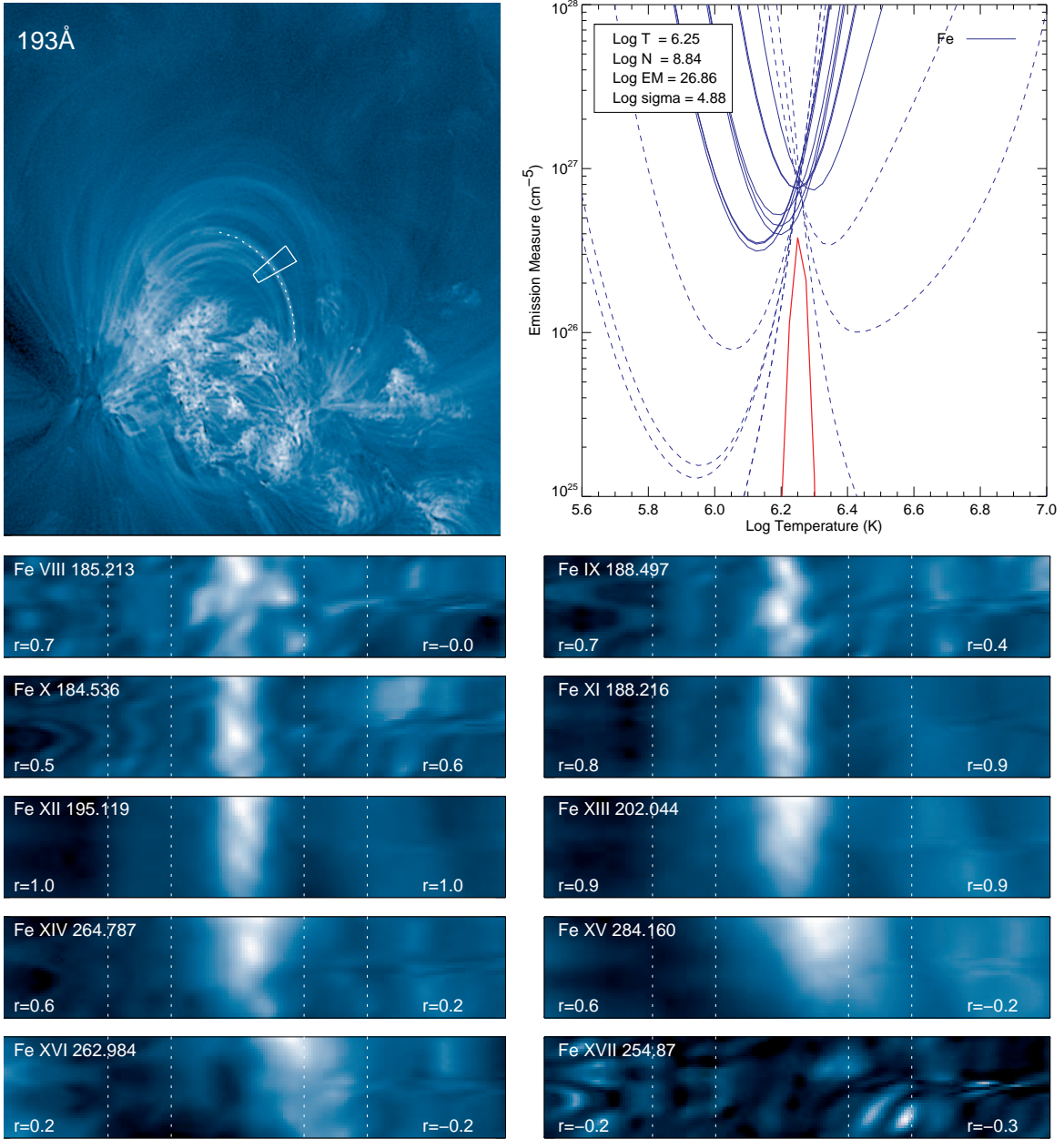


FIG. 1.— Images and emission measure distribution for the background around embedded loop #8. *Top Left*: AIA 193 Å image of the loop #8 environment. The dotted line shows the trace used to measure the loop half-length. The boxed region shows where the co-spatial background emission was measured. *Top Right*: The EM distribution for the co-spatial background. The blue curves are loci curves that indicate the constraints on the EM. Solid curves indicate spectral lines where the background emission is correlated with the background emission in Fe XII 195.119 Å. The dashed curves indicate spectral lines where the background emission is not correlated, and thus the intensities were set to zero. The red curve is the Gaussian EM distribution. The derived physical parameters are shown in the legend. *Lower Rows (2–6)*: Multi-wavelength images of the (straightened) embedded loop environment, also indicating the regions used for the cross-correlation analysis. The Pearson linear correlation coefficients ( $r$ ) for the left and right regions are also shown.

sities, loop widths, and cross-loop intensity profiles derived from both the EIS data and observations from AIA. The EIS observing sequence used the 1'' slit to scan an area of 240'' by 512'' in coarse 2'' steps. The sequence lasted about 2 hours and uses exposure times of 60s. The 4 additional examples were found after surveying data obtained using the same observing sequence through 2010–2012. We also used data from a narrower 120'' by 512'' scan that used 45s exposures and lasted around 45 mins. Both observing sequences recorded numerous strong spectral lines from the 180–285 Å

wavelength range. The data were then processed to remove instrumental effects, calibrated to physical units ( $\text{erg cm}^{-2} \text{s}^{-1} \text{sr}^{-1}$ ) and re-sampled to a 1'' scale. The SolarSoftware (SSW) routine `eis_prep` was used for the data processing.

For this work, the spectroscopic analysis of emission measures, densities, and temperatures was performed on the EIS data. We also, however, use 1.7–4s exposure 193 Å images from the AIA to measure the loop half-lengths. These data were processed for instrumental effects and made available online via the AIA cutout service. They are designated level

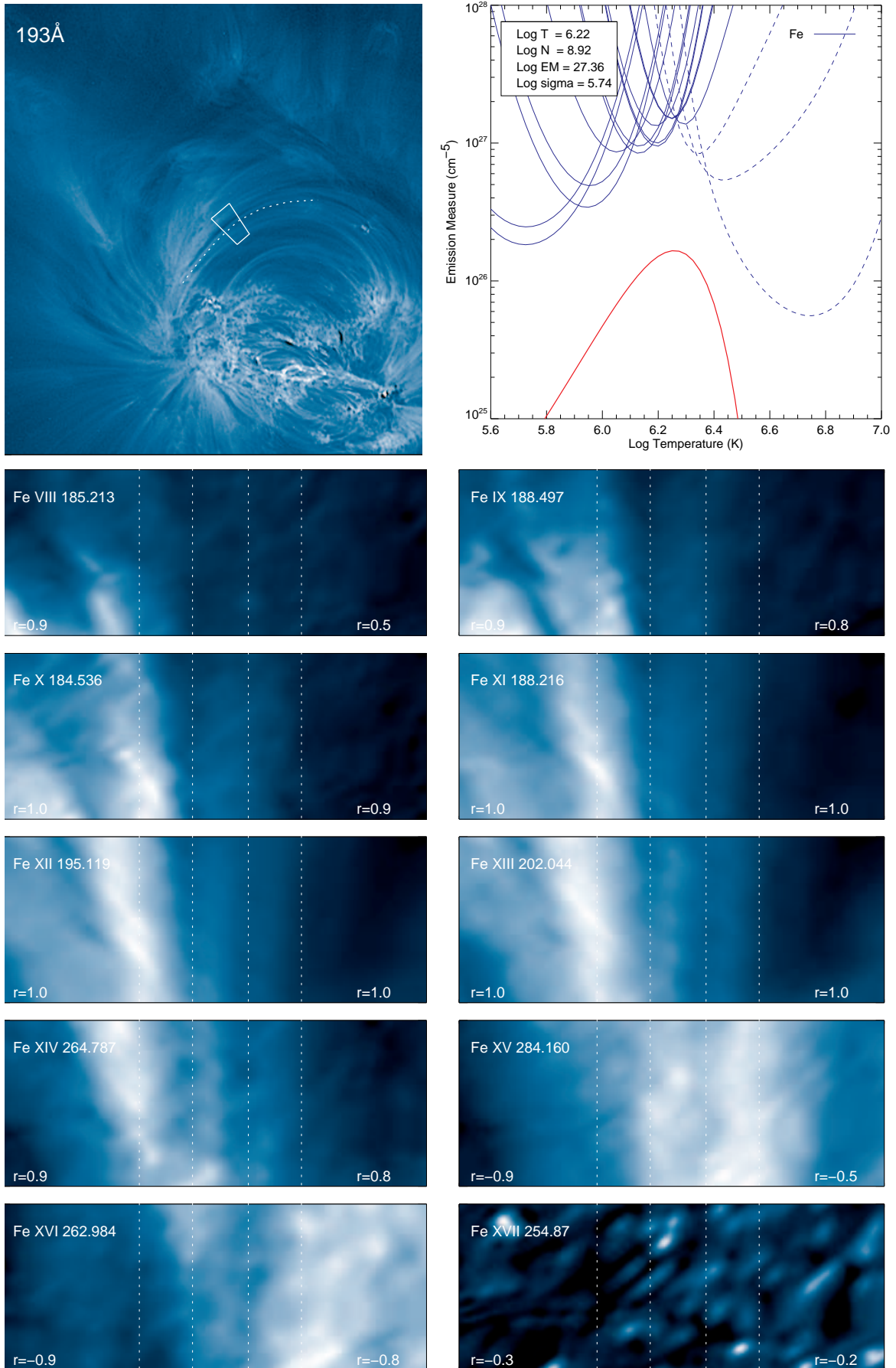


FIG. 2.— Same as Figure 1 but for the background around embedded loop #6.

1.5.

The EIS Fe XII 195.119 Å raster scan images were created by fitting the spectra at each pixel to a double Gaussian function that takes account of both the main line and the weaker blend at 195.18 Å. Prior to extracting the background intensities we also fit single or double Gaussian functions to the spectra at each pixel for all other wavelengths used in the analysis. For this study, we use the revised EIS intensity calibration of Warren et al. (2014).

To measure the co-spatial background to each loop we examined the cross-field loop intensity profile. We selected a clean portion of the loop, interpolated the intensities along the axis of the loop, straightened the loop, and averaged the intensities along the loop segment. We then used the averaged cross-loop intensity profile to visually identify two locations in the background close to the loop. We then fit the intensities between these locations with a first-order polynomial function. The measured background intensity is then the mean value of the polynomial function between the selected locations. The method is basically the same as established in Aschwanden et al. (2008) and Warren et al. (2008) except that we extract the background information rather than the loop information. We show examples of the chosen loop segments on AIA 193 Å images in Figures 1 and 2.

Also shown in Figures 1 and 2 are the traces used to measure the loop half-length. These measurements were made using the same loop tracing software but in this case we only recorded the dimensions of the straightened half-length segment. The loops were traced visually so there is some uncertainty in determining the loop footpoints and apex and in accounting for any projection effects. We will discuss the influence of the loop length on our conclusions in Section 3.

We applied this technique to the EIS Fe XII 195.119 Å data and then extended it to the other spectral lines using the same background locations. We need spectral lines from a broad range of temperatures to perform the EM analysis, so we used most of the strong lines from Fe VIII–Fe XVII that are observed by EIS. These are listed in Table 1 and we have used most of them successfully in previous emission measure studies (see e.g., Brooks & Warren 2011). At typical densities of the quiet Sun ( $\log(n/\text{cm}^{-3}) = 8.5$ , Brooks et al. 2009) these lines cover the temperature range 0.52–5.5 MK according to the CHIANTI v.8 database (Dere et al. 1997; Del Zanna et al. 2015).

We use CHIANTI v.8 to calculate all of the contribution functions we need for the EM analysis. The contribution function,  $G(T, n)$ , as a function of temperature ( $T$ ) and density ( $n$ ), is related to the observed line intensity for a transition between atomic levels  $i$  and  $j$  as

$$I_{ij} = \int G(T, n)\phi(T)dT \quad (1)$$

where  $\phi(T)$  is the differential emission measure re-cast as a function of temperature alone by assuming a fixed density at a given temperature. We use the Fe XIII 202.044/203.826 diagnostic line ratio to calculate the appropriate density in this work. We then fit the data with isothermal and Gaussian EM functions of the form

$$\phi(T) = EM_0\delta(T - T_0) \quad (2)$$

and

$$\phi(T) = \frac{EM_0}{\sigma_T\sqrt{2\pi}}\exp\left[-\frac{(T - T_0)^2}{2\sigma_T^2}\right] \quad (3)$$

TABLE 1  
EIS LINE-LIST USED FOR THE  
EMISSION MEASURE ANALYSIS.

Element	Ion	Wavelength/Å
Fe	VIII	185.213
Fe	VIII	186.601
Fe	IX	188.497
Fe	IX	197.862
Fe	X	184.536
Fe	XI	188.216
Fe	XI	188.299
Fe	XI	192.813
Fe	XII	186.880
Fe	XII	192.394
Fe	XII	195.119
Fe	XIII	202.044
Fe	XIII	203.826
Fe	XIV	264.787
Fe	XIV	270.519
Fe	XV	284.160
Fe	XVI	262.984
Fe	XVII	254.870

\* This is the complete list of lines used. They were not all used in the analysis of every dataset.

where  $EM_0$  and  $T_0$  are the peak emission measure and peak temperature, respectively, and  $\sigma_T$  is the Gaussian width of the EM distribution. We also compute the reduced  $\chi^2$  value for both models to allow a comparison of the quality of the fit. We use Equation 2 to test the isothermality of the plasma, and Equation 3 to detect any deviation from isothermal. The Gaussian EM has the advantage that if the plasma is multi-thermal, the width,  $\sigma_T$ , will increase, and this provides a good measure of the degree of multi-thermality. A fixed Gaussian EM of course does not give us any information on the true shape of the EM distribution, but this is not a significant issue for our study. We show examples of the EM analysis for two background regions in Figures 1 and 2. Figure 1 shows a case where the EM distribution is very close to isothermal, and Figure 2 shows a case where the EM distribution is somewhat broader.

For the EM analysis we also have to adopt some way to decide if the background emission at different wavelengths comes from the same structure. In loop analysis we usually only include lines if the cross-field intensity profile at that wavelength is highly correlated with the cross-field intensity profile at the wavelength used to identify the loop. Here we looked at the spatial distribution of intensity in the straightened image segment, parallel to the loop and within 5 pixels on either side. If the linear Pearson correlation coefficient,  $r$ , between the spatial distribution of intensity on either side of the loop and the spatial distribution of intensity in the corresponding region of the Fe XII 195.119 Å image was greater than 0.75, then that wavelength was included. Figures 1 and 2 also show examples of the embedded loop environment at different wavelengths and the background regions chosen for the cross-correlation analysis. We allow either side to be correlated because although we have tried to find clean isolated loop segments, there is a natural transition in the structure of active regions as a function of temperature that tends to favour excluding cooler lines on the inside of loop arcades and hotter lines on the outside. Figure 1 shows this effect for the cooler Fe VIII 185.213 Å line. The Fe XII 195.119 Å emission on the outside of the loop in Fe VIII 185.213 Å is correlated with



the emission on the outside of the Fe XII 195.119 Å loop ( $r=0.7$ ), but the emission on the inside is uncorrelated ( $r=0.0$ ) because of the presence of hot core emission that is not seen at the temperatures of Fe VIII 185.213 Å but has an increasing contribution at the temperatures of Fe XII 195.119 Å. Our method therefore may have a tendency to include more spectral lines in the analysis. If the emission on neither side of the loop is highly correlated then the intensity is set to zero and the error is set to 22% of the background measurement (the approximate intensity calibration error, Lang et al. 2006).

### 3. RESULTS AND DISCUSSION

We give the results for the complete analysis of all 24 background regions in Table 2. The table shows the dates and times of all the observations we analyzed, together with a comparison of the  $\chi^2$  values for the isothermal and Gaussian EM analysis and the electron density evaluated from the Fe XIII ratio. The  $\chi^2$  for the Gaussian model is closer to one in 88% of the regions so we conclude that only three regions are likely isothermal. Since the Gaussian model is a better fit in general, we only report the peak temperature, peak EM, and thermal width from this model. Despite this, about half the regions (11/24) have narrow thermal widths that are less than  $\log(T/K) = 5$  ( $7.6 \times 10^4$  K). Their peak temperatures fall in the range  $\log(T/K) = 6.16\text{--}6.31$  (1.4–2 MK). Conversely, most of the other regions (9/13) have thermal widths greater than  $\log(T/K) = 5.5$  ( $3 \times 10^5$  K), and their peak temperatures are  $\log(T/K) = 6.2\text{--}6.5$  (1.6–3.2 MK). The densities for all the regions are comparable. They fall in the range  $\log(n/\text{cm}^{-3}) = 8.5\text{--}9.0$ .

The temperatures and densities for the background regions with narrow temperature distributions agree well with the previous results of Del Zanna & Mason (2003) and Subramanian et al. (2014), but the thermal width is much narrower, and hence the EM slopes are steeper. This is likely a result of only including background emission that is correlated with the emission at the temperature of Fe XII 195.119 Å.

Regions with broader temperature distributions and higher peak temperatures (up to 3 MK), however, have not been discussed in this context before. Recall that this is diffuse emission around high lying warm loops, and it is not clear if this is equivalent to the background emission around hot, compact core loops, though it seems likely that this diffuse emission envelops the whole active region. That conjecture is supported by the work of Subramanian et al. (2014), who report that the diffuse emission above the active region core shows characteristics similar to the hot core itself.

Our results for the background emission around warm loops are also similar to the results for coronal loops. Background emission peaked near 1.7 MK has a narrow temperature distribution, but is generally not isothermal. The higher temperature background emission has a broader temperature distribution. In fact, the width of the thermal distribution strongly correlates with the peak temperature. We plot the two quantities against each other in Figure 3. The linear Pearson correlation coefficient is  $r = 0.74$ . This result is similar to that reported for coronal loops by Schmelz et al. (2014), who argued that the loop emission measure distribution may narrow as it cools.

As discussed in the introduction, background subtraction is critical for measuring the properties of the loops themselves (Klimchuk et al. 1992; Del Zanna & Mason 2003). In this sample of loops, there is only one example where the back-

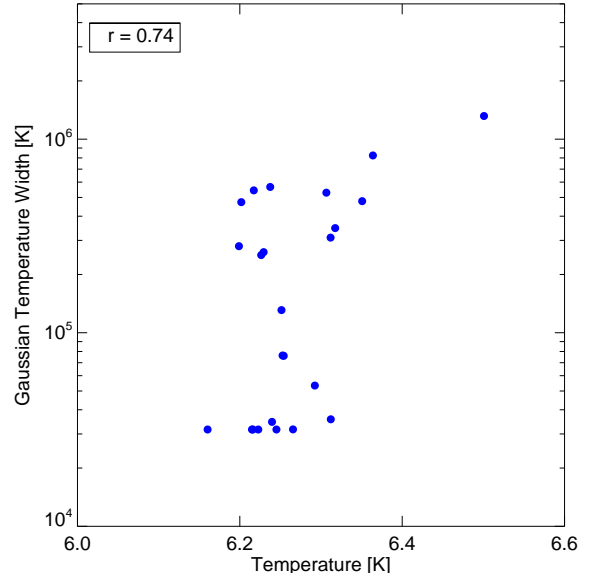


FIG. 3.— The relationship between peak temperature and the emission measure (Gaussian) width for the sample of diffuse background measurements.

ground emission is comparable in the two Fe XIII lines used for measuring the electron densities. In the rest of the sample, not removing the background results in density changes of at least 40%, rising to a maximum of a factor of 3.7. On average, densities would be a factor of  $\sim 2$  lower if the background were not subtracted. Since the measurement is an average of the background and loop intensity observed along the line of sight, this intuitively suggests that densities in the background emission should be lower. This is exactly what we find in our analysis and is potentially significant. Densities in the background are less than  $\log(n/\text{cm}^{-3}) = 9$ , whereas warm loops generally have densities above  $\log(n/\text{cm}^{-3}) = 9$  (see, e.g., Brooks et al. 2012).

These results suggest that the background plasma may be closer to static equilibrium. As discussed in Section 1, by measuring the background co-spatially with warm loops we have a better measurement of the emission in which the loops are truly embedded. Therefore, we can make some assumption about the background field lengths based on the embedded loop length, and this allows us to make a direct comparison with coronal loop scaling laws. As a first step in making some progress on the topic in this paper, we simply assume that the background field length is the same as the measured loop length. This allows us to calculate the column density,  $nL$ .

Figure 4 shows the relationship between the measured temperature and column density for the diffuse background data points (blue). We also show the corresponding values for the loops embedded in the background (red). Also plotted on the graph are two theoretical scaling laws. The solid line is the well-known RTV law (Rosner et al. 1978). Strictly speaking this scaling relates the maximum temperature of the loop to the column density assuming the heat source is located at the loop top. The dotted line is the scaling law assuming that the heating occurs uniformly along the loop (Kano & Tsuneta 1995). Note that in our loop sample not all of our measurements are made at the loop top, and may also not be located at the loop maximum temperature. The locations were chosen to get a clean cross-field intensity profile for a different

TABLE 2  
 EIS MEASUREMENTS OF THE DIFFUSE BACKGROUND EMISSION.

#	Date/Time	ELH	$\chi_i^2$	$\chi_g^2$	$T$	$n$	EM	$\sigma_T$	#	Date/Time	ELH	$\chi_i^2$	$\chi_g^2$	$T$	$n$	EM	$\sigma_T$
1	01/21 13:57	20.9	1.05	1.15	6.22	8.99	26.8	4.50	11	04/29 01:23	35.8	1.49	1.25	6.23	8.77	27.0	5.40
2	01/30 20:11	36.9	5.55	1.35	6.20	8.86	27.1	5.67	12	05/06 13:55	19.4	2.60	1.16	6.31	9.03	27.2	5.72
3	03/18 09:34	62.6	0.63	0.69	6.25	8.70	26.9	4.50	13	06/14 00:52	29.9	0.75	0.78	6.25	8.89	26.9	5.12
4	03/18 11:05	55.0	1.06	1.15	6.16	8.65	27.0	4.50	14	07/02 03:32	28.0	0.78	0.86	6.27	8.88	26.9	4.50
5	04/15 00:41	61.4	4.27	1.93	6.36	8.99	27.6	5.92	15	07/02 03:53	38.8	1.47	1.60	6.29	8.82	27.0	4.73
6	04/15 01:41	79.6	5.07	1.08	6.22	8.92	27.4	5.74	16	09/02 13:25	68.9	0.78	0.84	6.25	8.85	27.1	4.88
7	04/21 12:02	25.6	1.16	0.88	6.31	8.74	26.9	5.49	17	09/02 13:54	35.0	0.73	0.79	6.24	8.69	26.9	4.54
8	04/21 12:18	58.7	0.59	0.63	6.25	8.84	26.9	4.88	18	09/17 18:57	44.6	8.67	1.38	6.50	9.03	27.6	6.12
9	04/22 08:56	44.0	1.26	0.85	6.32	8.86	27.3	5.54	19	10/14 22:55	119.8	0.90	0.98	6.21	8.76	26.5	4.50
10	04/22 09:00	34.7	0.89	0.97	6.22	8.94	26.9	4.50	20	10/14 23:51	24.6	4.09	2.56	6.35	8.74	27.4	5.68
-	10/09/05 04:10	124.1	2.65	1.13	6.20	8.46	27.1	5.45	-	06/27 12:08	80.7	7.15	0.58	6.24	8.79	27.6	5.75
-	06/27 12:14	80.0	0.75	0.82	6.31	8.63	27.4	4.55	-	12/05/16 23:52	68.5	1.95	1.27	6.23	8.64	27.2	5.42

\* The index indicates the loop number from Brooks et al. (2012) for comparison. Additional new loops are unnumbered. All loops were observed in 2011 except where indicated. The EIS slit passed over the loop segment at the given date and time. *ELH* is the half length of the loop embedded in the background emission.  $\chi_i^2$  and  $\chi_g^2$  are the reduced chi squared values for the isothermal and Gaussian models, respectively.  $T$ ,  $n$ , *EM*, and  $\sigma_T$  are the emission measure peak temperature, electron density, peak emission measure, and (Gaussian) emission measure width, respectively. The physical parameters are all from the Gaussian emission measure model.

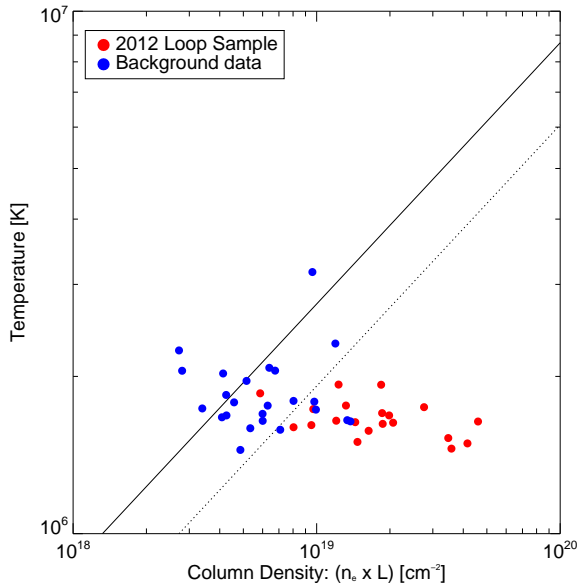


FIG. 4.— The relationship between measured temperature,  $T$ , and column density,  $(nL)$ , for the diffuse background (blue) and a sample of coronal loops (red) from Brooks et al. (2012). The solid and dotted lines are theoretical scaling laws:  $1.4 \times 10^3 (pL)^{1/3}$  (RTV - solid) and  $1.1 \times 10^3 (pL)^{1/3}$  (dotted).

purpose. We only show these data points, for comparison, however. With no discernible structure, it is not possible to verify the top of the background emission.

The Figure shows the well known result that warm loops are over-dense quite clearly. While a few of the warm loops might be said to agree with the uniform heating scaling law, the mean loop density is  $\log(n/\text{cm}^{-3}) = 9.4$  at the mean temperature of 1.7 MK, and this is about a factor of 5.4 larger than the expected density from the RTV scaling law, and a factor of 2.6 larger than the expected density from the uniform heating scaling law. In contrast, most of the background emission appears broadly consistent with one or other of the scaling laws. The densities of 10/24 regions are within 40% of the expected values from the RTV scaling law, and 10 others are within 40% of the expected values from the uniform heating law. Only 2/24 are under-dense compared to the RTV scaling prediction - again similar to some reports of densities in the high temperature core emission (Winebarger et al. 2003;

Klimchuk 2006) - and two others are over-dense compared to the uniform heating law.

We recognize that our simple assumption about the field line length is an approximation that affects these results. There are a few background regions where the agreement with static theory would begin to break down if the field lines were  $\sim 30\text{--}50\%$  longer. Since the mean background density is  $\log(n/\text{cm}^{-3}) = 8.8$  and the mean temperature is 1.9 MK, however, the field line lengths would have to be factors of 2–3 longer on average to produce a similar disagreement with theory to that which is seen for the warm loops. We do not expect that our loop length measurements are inaccurate to this degree, but of course we cannot rule out some unexpected property of the background field that means it does not track the loop closely, e.g., if it reaches much higher altitudes near the apex, or if the eccentricity is lower than for the loop and the separation between footpoints is much greater. These factors, however, lead to several cases where the loop length approaches the largest in our sample (half-length of 120 Mm), and, assuming a circular loop, footpoint separations of  $>200''$ . These dimensions are typical only of the largest active regions.

Conversely, we know that the emission we measure is an integrated total along the line-of-sight, and the path length is likely to be quite large. Estimates assuming an isothermal plasma and an exponential fall-off in density with a hydrostatic scale-height suggest that the path length needs to be 160–200 Mm to encompass 80% of the emission along the line-of-sight (Aschwanden & Acton 2001; Warren & Warshall 2002; Brooks & Warren 2008). This will of course include emission from both large-scale overlying foreground magnetic field, and small-scale background field. It would be interesting to model the background magnetic field and determine whether the integrated line-of-sight intensity is dominated by emission from an ensemble of field lines with an average length close to that of the embedded loop. While at first sight this may appear unlikely, it also seems unlikely that it would be dominated by only the largest scale magnetic field because the emission is dropping with height, and this is what is needed to break the agreement with the static loop scaling laws (based on the simple assumption that the field length is comparable to the embedded loop length).

In summary, we have studied the densities and temperatures of a sample of 24 diffuse background/foreground emission regions that are co-spatial with embedded warm loops,

and where the emission at different temperatures comes from the same structures (based on our cross-correlation analysis). By analyzing the co-spatial background we obtain results that are more representative of the embedded loop environment, and we are also able to use the loop information to guide assumptions about the length of the background field. In this way we were able to compare the background properties to expectations from static loop scaling laws. The results we present here suggest that the properties of the majority of the background regions in our sample are compatible with quasi-steady, or high frequency impulsive heating.

DHB would like to thank Harry Warren for helpful comments on the manuscript. The work of DHB was performed

under contract to the Naval Research Laboratory and was funded by the NASA *Hinode* program. *Hinode* is a Japanese mission developed and launched by ISAS/JAXA, collaborating with NAOJ as a domestic partner, NASA and STFC (UK) as international partners. Scientific operation of the *Hinode* mission is conducted by the *Hinode* science team organized at ISAS/JAXA. This team mainly consists of scientists from institutes in the partner countries. Support for the post-launch operation is provided by JAXA and NAOJ(Japan), STFC (U.K.), NASA, ESA, and NSC (Norway). Courtesy of the NASA/SDO, and the AIA, EVE, and HMI science teams. CHIANTI is a collaborative project involving George Mason University, the University of Michigan (USA) and the University of Cambridge (UK).

#### REFERENCES

- Aschwanden, M. J. 2001, ApJ, 559, L171  
 Aschwanden, M. J., & Acton, L. W. 2001, ApJ, 550, 475  
 Aschwanden, M. J., & Nightingale, R. W. 2005, ApJ, 633, 499  
 Aschwanden, M. J., Nitta, N. V., Wuelser, J., & Lemen, J. R. 2008, ApJ, 680, 1477  
 Aschwanden, M. J., Schrijver, C. J., & Alexander, D. 2001, ApJ, 550, 1036  
 Brooks, D. H., & Warren, H. P. 2008, ApJ, 687, 1363  
 Brooks, D. H., & Warren, H. P. 2009, ApJ, 703, L10  
 Brooks, D. H., & Warren, H. P. 2011, ApJ, 727, L13  
 Brooks, D. H., Warren, H. P., & Ugarte-Urra, I. 2012, ApJ, 755, L33  
 Brooks, D. H., Warren, H. P., Williams, D. R., & Watanabe, T. 2009, ApJ, 705, 1522  
 Cirtain, J., Martens, P. C. H., Acton, L. W., & Weber, M. 2006, Sol. Phys., 235, 295  
 Culhane, J. L., et al. 2007, Sol. Phys., 243, 19  
 Del Zanna, G. 2003, A&A, 406, L5  
 Del Zanna, G. 2012, A&A, 537, A38  
 Del Zanna, G. 2013, A&A, 558, A73  
 Del Zanna, G., Dere, K. P., Young, P. R., Landi, E., & Mason, H. E. 2015, A&A, 582, A56  
 Del Zanna, G., & Mason, H. E. 2003, A&A, 406, 1089  
 Dere, K. P., Landi, E., Mason, H. E., Monsignori Fossi, B. C., & Young, P. R. 1997, A&AS, 125, 149  
 Handy, B. N., et al. 1999, Sol. Phys., 187, 229  
 Harrison, R. A., et al. 1995, Sol. Phys., 162, 233  
 Kano, R., & Tsuneta, S. 1995, ApJ, 454, 934  
 Klimchuk, J. A. 2006, Sol. Phys., 234, 41  
 Klimchuk, J. A., Lemen, J. R., Feldman, U., Tsuneta, S., & Uchida, Y. 1992, PASJ, 44, L181  
 Lang, J., et al. 2006, Appl. Opt., 45, 8689  
 Lemen, J. R., et al. 2012, Sol. Phys., 275, 17  
 Lenz, D. D., Deluca, E. E., Golub, L., Rosner, R., & Bookbinder, J. A. 1999, ApJ, 517, L155  
 Pesnell, W. D., Thompson, B. J., & Chamberlin, P. C. 2012, Sol. Phys., 275, 3  
 Polito, V., Testa, P., Allred, J., Pontieu, B. D., Carlsson, M., Pereira, T. M. D., Goi, M., & Reale, F. 2018, The Astrophysical Journal, 856, 178  
 Porter, L. J., & Klimchuk, J. A. 1995, ApJ, 454, 499  
 Priest, E. R., Foley, C. R., Heyvaerts, J., Arber, T. D., Culhane, J. L., & Acton, L. W. 1998, Nature, 393, 545  
 Reale, F. 2002, ApJ, 580, 566  
 Reale, F. 2014, Living Reviews in Solar Physics, 11, 4  
 Rosner, R., Tucker, W. H., & Vaiana, G. S. 1978, ApJ, 220, 643  
 Schmelz, J. T., Pathak, S., Dhaliwal, R. S., Christian, G. M., & Fair, C. B. 2014, ApJ, 795, 139  
 Schmelz, J. T., Scopes, R. T., Cirtain, J. W., Winter, H. D., & Allen, J. D. 2001, ApJ, 556, 896  
 Subramanian, S., Tripathi, D., Klimchuk, J. A., & Mason, H. E. 2014, ApJ, 795, 76  
 Testa, P., et al. 2013, ApJ, 770, L1  
 Tripathi, D., Klimchuk, J. A., & Mason, H. E. 2011, ApJ, 740, 111  
 Ugarte-Urra, I., & Warren, H. P. 2012, ApJ, 761, 21  
 Viall, N. M., & Klimchuk, J. A. 2011, ApJ, 738, 24  
 Viall, N. M., & Klimchuk, J. A. 2012, ApJ, 753, 35  
 Viall, N. M., & Klimchuk, J. A. 2017, ApJ, 842, 108  
 Warren, H. P., Brooks, D. H., & Winebarger, A. R. 2011, ApJ, 734, 90  
 Warren, H. P., Ugarte-Urra, I., Doschek, G. A., Brooks, D. H., & Williams, D. R. 2008, ApJ, 686, L131  
 Warren, H. P., Ugarte-Urra, I., & Landi, E. 2014, ApJS, 213, 11  
 Warren, H. P., & Warshall, A. D. 2002, ApJ, 571, 999  
 Warren, H. P., Winebarger, A. R., & Brooks, D. H. 2012, ApJ, 759, 141  
 Winebarger, A. R. 2012, in Astronomical Society of the Pacific Conference Series, Vol. 456, Fifth Hinode Science Meeting, ed. L. Golub, I. De Moortel, & T. Shimizu, 103  
 Winebarger, A. R., Schmelz, J. T., Warren, H. P., Saar, S. H., & Kashyap, V. L. 2011, ApJ, 740, 2  
 Winebarger, A. R., Warren, H. P., & Mariska, J. T. 2003, ApJ, 587, 439